Full length article

Machine learning based hierarchy of causative variables for tool failure in friction stir welding

Y. Du[a,b], T. Mukherjee[a], P. Mitra[c], T. DebRoy[a,*]

[a] Department of Materials Science and Engineering, Pennsylvania State University, University Park, PA 16802, USA
[b] Tianjin Key Laboratory of Advanced Joining Technology, School of Materials Science and Engineering, Tianjin University, Tianjin 300350, China
[c] College of Information Sciences and Technology, Pennsylvania State University, University Park, PA 16802, USA

ABSTRACT

Since friction stir welding tools fail in service under various mechanisms, it is difficult to mitigate tool failure based on mechanistic understanding alone. Here we use multiple machine learning algorithms and a mechanistic model to identify the causative variables responsible for tool failure. We analyze one hundred and fourteen sets of experimental data for three commonly used alloys to evaluate the hierarchy of causative variables for tool failure. Three decision tree based algorithms are used to rank the hierarchy of the relative influence of six important friction stir welding variables on tool failure. The maximum shear stress is found to be the most important causative variable for tool failure. This is consistent with the effect of shear stress on the load experienced by the tool. The second most important factor is the flow stress which affects the plasticized material flow around the tool pin. All other variables are found to be significantly less important. Three algorithms also generate identical results and predict tool failure with the highest accuracy of 98%. A combination of mechanistic model, machine learning and experimental data can prevent tool failure accurately.

© 2020 Acta Materialia Inc. Published by Elsevier Ltd. All rights reserved.

1. Introduction

In friction stir welding (FSW) process, tools are exposed to high stresses and temperatures. Temperature fields and stresses on the tool affect the structure and properties of the joints and in extreme conditions, results in tool failure that disrupts the joining process [1–7]. Several mechanisms of tool failure have been reported in the literature based on welding conditions. Tools experience fluctuating tensile and compressive loads because of their rotational and translational motion through the plasticized workpiece. Prolonged exposure of the tool to high fluctuating stresses may result in fatigue failure [5]. Since the yield strength decreases with increase in temperature, tools often deform at high loads and temperatures [8]. Shear failure occurs when the stresses on the tool pin are higher than its load bearing ability [8]. At high temperatures, alloying elements in the workpiece may diffuse into the tool and form brittle intermetallic compounds which weakens the tools [9,10]. The rotational and translational motions of tool through the hot plasticized material result in its wear and pronounced wear may also result in tool failure [1,5]. In practice, FSW tools may fail because of multiple mechanisms and there is no unified, phenomenological criterion to determine the most important variables that can be adjusted to prevent tool failure.

Several investigations have been undertaken to identify the conditions for tool failure [8–26]. The improper material flow and overloading of tools at high welding speeds often result in tool failure. Peak temperature affects the tool properties and is recognized as a factor for tool durability [11–15]. Discontinuous material flow in the weld nugget at high strains and strain rates was reported to be detrimental to the tool [16–19]. The flow stress was suggested as an important causative factor for tool breakage since high flow stress indicates difficulty of material flow [5,20–22]. Improper conditions of material flow that generate high traverse force, torque and shear stress on the tool have been suggested as the main reasons for tool failure [1,4,23–28]. Insufficient heat generation and excessive plunge depth were also thought to be important factors. Sufficient distance between the tool pin tip and the bottom surface of work plate was necessary to protect tools from contacting the work bench and tool failure [1,5]. It was found that the tool breakage was more common at high weld pitch (welding speed to rotational speed ratio) [29]. Undesirable hard secondary phases formed during welding were found to be the main reasons for tool wear [9,10]. Tools with high fracture toughness, excellent yield strength and wear resistance at high temperature were suggested to be helpful to reduce tool failure [11].

The most important causative variables and their hierarchical influence on tool failure are not available in the literature. Data-driven machine learning techniques are often beneficial to establish relations among different sets of variables when phenomenological relations among them are unavailable [4,30–37]. In data-driven

machine learning methods, the raw process variables are the most convenient inputs because they can be obtained easily and recorded directly during the experiments [38]. In addition, engineers can easily control these variables in order to achieve desired product attributes and tool life. However, the raw process variables are distributed over a very large range in a complex system such as FSW where the effects of individual parameters are concealed by the complexity of plasticized material flow and load on tool that affect the tool failure. Therefore, use of computed variables rather than raw process variables are more useful in a multi-variables system like FSW [4]. These complex variables are often referred as causative variables because they affect tool failure. The importance of causative variables compared to the raw individual variables is evident in a parallel, well-recognized example of fluid flow through a pipe. The raw variables such as the diameter of the pipe, average velocity, density and viscosity of the fluid can determine whether the flow is turbulent or laminar [39]. However, the flow behavior is much better indicated by the Reynolds number than the four individual parameters [39]. Therefore, here we consider both the raw variables as well as the causative variables that represent the flow of plasticized material and load on tool. The raw variables considered here are the welding process parameters, tool and work plate dimensions and material properties of the work plate. Since the same tool material, H13 tool steel, is used for these three aluminum alloys, the tool properties are not included in the raw variables. The causative variables, temperature, strain rate, flow stress of plasticized material as well as traverse force, torque and maximum shear stress on the tool are estimated using a well-tested, 3D, heat transfer and material flow model [2,42]. The model is rigorously tested using independent experimental data of temperature field [43] as well as forces and torques on tools [44] for various welding conditions. A binary variable is used as output for the machine learning algorithms: '1' for 'Broken tool' and '0' for 'Safe tool' output.

Here we train, test and validate neural network (NN) and decision tree (DT) using both raw and causative variables based on one hundred and fourteen sets of experimental data for three aluminum alloys, AA2219 [29], AA5083 [40] and AA6082 [41] from peer-reviewed literature. All experimental data used in this investigation are for premature tool failure due to improper processing conditions. The effectiveness of the machine learning algorithms in predicting tool breakage using the six causative variables is compared with that using raw welding parameters and alloy properties. The hierarchical influence of these causative variables on tool failure is also estimated using three feature selection indexes-based machine learning. However, the hierarchical influence of the raw variables on tool failure cannot be estimated because these parameters show nearly the same effect on tool failure. In other words, if any one of these variables is kept constant, alteration of the other variables may cause both 'Safe tool' and 'Broken tool'. Although the method we propose in this research is applied for the FSW of aluminum alloys, it is equally applicable for the FSW of other alloys such as steels when experimental data becomes available in the literature.

2. Methodology

The methodology for this research is schematically represented in Fig. 1. Two types of datasets are used in machine learning as input. First, the raw unprocessed welding parameters are used that are easy to measure and available from literature directly. Second, the six causative variables calculated using a 3D, heat transfer and material flow model [4,42] are used in the machine learning. Both the sets of data are for one hundred and fourteen independent experiments on tool failure adapted from the literature [29,40,41]. Two machine learning algorithms, neural network (NN) and decision tree (DT) [4,30,37] are used in this research. The detailed calculations of six causative variables using the numerical model and machine learning algorithms are described below.

2.1. Calculations of six causative variables

The six causative variables investigated in this paper are calculated using a three-dimensional heat transfer and visco-plastic flow model [2,8,42]. The model solves the equations of conservation of mass, momentum, and energy in 3D Cartesian coordinate [2,8,42]. The temperature and velocity fields can be computed combined with the velocity and heat transfer boundary conditions. The strain rate is defined as the velocity gradient and calculated in the weld nugget [16]. The flow stress for the plasticized material flow can be computed with the effective strain rate and temperature field [2]. Since, flow stress varies spatially in 3D, maximum value of flow stress is used in machine learning. The spatial variations of fractional slip (δ) and the coefficient of friction (μ_f) are estimated based on the rotational speed and tool geometry [8]. The traverse force is opposite to the welding direction. F_S and F_P are the force components experienced by the tool pin and the shoulder respectively which can be calculated as:

$$F_S = \oint \delta \times \mu_f P \times d_A \tag{1}$$

$$F_P = \oint \sigma \times d_A \tag{2}$$

where δ and μ_f are the fractional slip and friction coefficients. P is the axial pressure. The σ is the temperature-dependent yield strength of the plasticized flow material and d_A is the area on the tool that contacted with the plasticized material.

The torque that tool sustains is related to both the sticking torque and the sliding torque, and the relationship is described in a previous paper [8]. The torque generated by the shoulder is higher than that caused by the tool pin because the diameter of shoulder is larger than that of tool pin [3,8]. With the distribution of force and torque on the tool pin, the shear stress due to bending and torsion loading can be computed at any point on the tool pin. The maximum and minimum principal stresses can be estimated. The variation of maximum shear stress around the tool pin can be obtained from Tresca's criteria described in the literature [1,8].

2.2. Implementation of machine learning

2.2.1. Data classification and oversampling to avoid bias in dataset

One hundred and fourteen sets of independent FSW experimental data on tool failure of three commonly used aluminum alloys, AA2219, AA5083 and AA6082 were collected from the peer-reviewed literature [29,40,41]. Two machine learning approaches [30], neural network (NN) and decision tree (DT), were employed to classify the datasets for tool failure. Among all one hundred and fourteen data points, 91 of them were 'Safe tool' marked with '0', and the remaining 23 were 'Broken tool' marked with '1'. For 91 cases of 'Safe tool', 55 of them were selected randomly for the training, 9 for the validation and the remaining 27 for testing. Oversampling [30] was applied to increase the number of 'Broken tool' cases from 23 to 92 to make the dataset unbiased. For the 92 cases of 'Broken tool', 56 of them were selected randomly for the training, 9 and 27 were chosen for the validation and testing respectively. In total, 111 data points were applied for training, 18 for validation and 54 for testing.

2.2.2. Machine learning algorithms

In the NN, all training data were used to fit a hyperbolic tangent function by using error back-propagation algorithm that minimizes the logarithmic error to update the weights linking different layers [37]. The number of hidden nodes was set to vary from n to $2n$ (n is the number of input nodes). The aim of training is to find the best weight matrix with least error between the predictive response and target response. The computed best weight matrix was supposed to apply for validation and testing datasets. The structure and weight matrix for neural
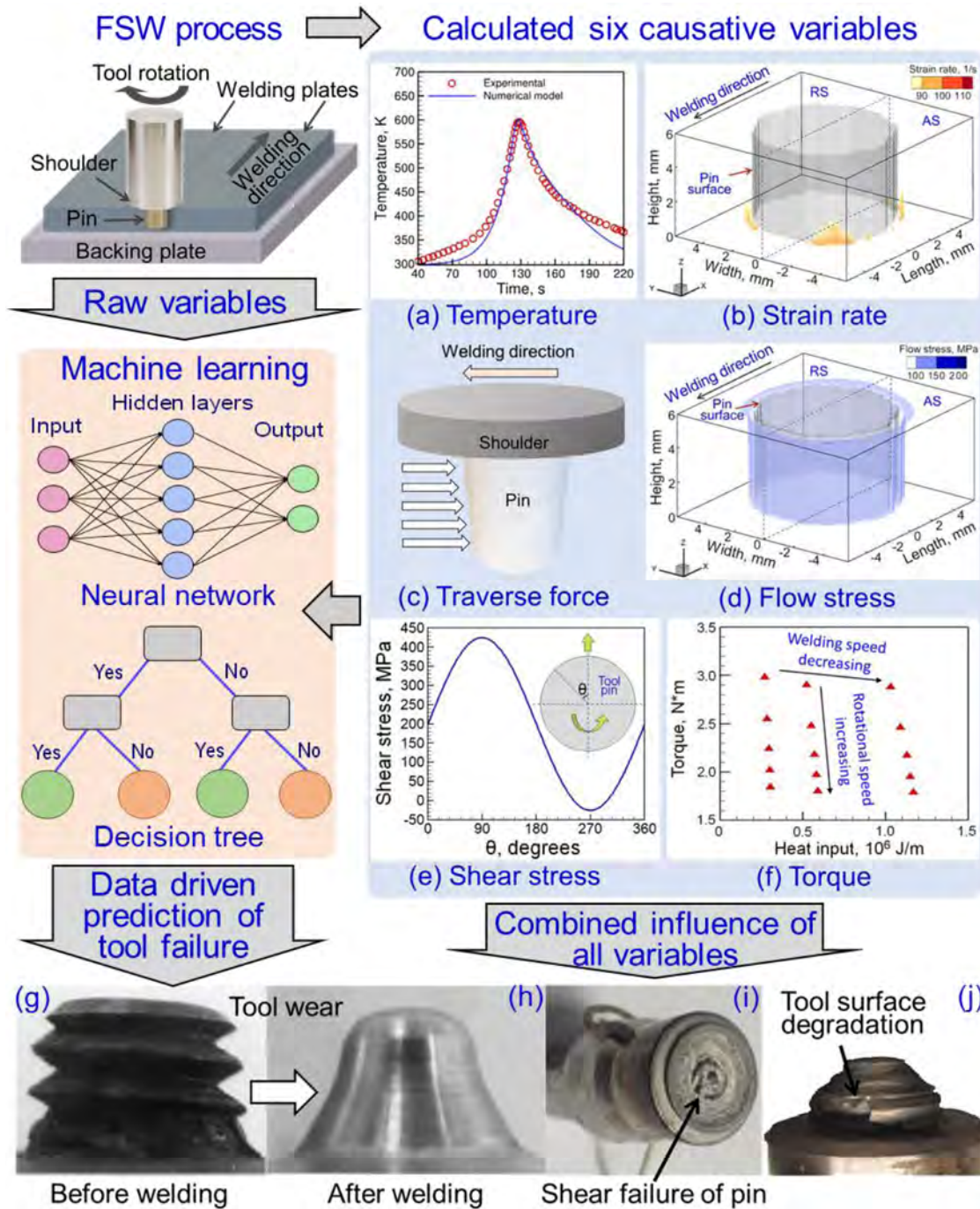
Fig. 1. This schematic outlines the structure of this research. The essential components are FSW process, numerical model and machine learning methods including neural network and decision tree. Numerical model is used to calculate the six causative variables (a) temperature (b) strain rate (c) traverse force (d) flow stress (e) shear stress (f) torque. The images of tool in figures (g-j) are taken from the literature [5,9,11].

network is explained in the Supplementary Information. The outputs of NN training were continuous values between 0 and 1, which need to be separated by selecting a proper threshold value. The best value of the threshold with the highest accuracy in evaluating training output, was also used to clarify the validation output and testing output. The output node was estimated using the following function [4,30,37].

$$y = \tanh\left(\sum_{i=1}^{n} w_i x_i + \theta_i\right) \quad (3)$$

where n is the total number of input nodes, w_i is the weight between the input nodes and hidden nodes, x_i and y are the input and the output of a node, θ_i is the bias dependent on the ith input.

There are three commonly used algorithms for making a decision tree, ID 3, C4.5 and CART (classification and regression tree) that use three different feature importance indexes, information gain (IG), information gain ratio (IG ratio) and Gini index, respectively [30]. These three indexes can represent the global feature importance of six causative variables using all data points. The hierarchical importance of these six causative variables are ranked by the above-mentioned three indexes and a decision tree is generated to predict tool failure [4,30]. The basic structure of DT is '$x_i > p$' where x_i is the root or child node and p is the threshold value. The selection of threshold value is as same as the threshold value selection in NN. The best value of the threshold with the least classification error was selected to

classify the datasets. For example, for ID 3 algorithm, the selection of classification nodes were performed based on the information gain (IG) [30,31]. The variable that had the highest information gain was selected as the node for each ranking. After the first-time ranking, select the root node with the highest IG value, and chose the best threshold value with highest classification accuracy, and then classify the dataset into two groups with the remaining variables [4,30]. The above operation needs to be repeated until the leaves of the tree are reached. The process to construct a decision tree using ID 3 algorithm is described in the Supplementary Information.

3. Results and discussion

A significant effort was made to correlate the raw welding variables with the tool failure. The raw, unprocessed variables include welding and rotational speeds, axial pressure, tilt angle, shoulder radius, pin radius, plate thickness, work plate material properties of thermal diffusivity and yield strength. The same tool material, H13 tool steel is used for all the one hundred and fourteen cases. Therefore, the material properties of tool material are not included in the raw variables. These variables corresponding to one hundred and fourteen experiments are adapted from the literature and are listed in the Supplementary Information. The weight matrix for NN using raw weld parameters are provided in the Supplementary Information. This method predicts tool failure with an accuracy of 87.0%. This average accuracy in prediction is primarily attributed to the fact that the raw, unprocessed welding variables alone are inadequate to explain complex phenomena such as tool failure in FSW. In many complicated engineering systems, some complex variables which combine the simultaneous influence of several variables are better suited than the raw individual parameters to represent the behavior of the system. These variables are often termed as causative variable because they are good representative of the causative factors of tool failure. Therefore, we used the six potentially

causative variables to try to achieve a significantly improved reliability in predicting tool failure. Since these causative variables cannot be recorded in shop floor during experiments, this procedure requires the calculations of the variables using the heat transfer and material flow model [2,42]. The calculated results to explain the influence of the six variables on tool failure and their validations using independent experimental data are described below.

3.1. Calculated results of six variables and experimental validations

Fig. 2(a) shows the calculated 3D distribution of the temperature field. The color bands in this figure represent the range of temperatures as indicated in the contour legend. The temperature is the maximum near the tool pin and gradually decreases away from the pin. The isotherms are elongated at the rear side of the tool pin opposite to the welding direction. This unique temperature distribution affects both the load generated on the tool and its load bearing ability. For example, materials at high temperature are more plastic, easy to flow and therefore generate less load on tool pin [2,5,7]. In contrast, high temperature degrades the load bearing ability of the pin [1,5,8]. Because of these influences, temperature is considered to be a potential causative variable for tool failure. To check the accuracy of the calculated temperature values the computed results are compared against the independent experimental data. Fig. 2(b) shows that the computed temperature-time curve shows a good agreement with the experimental results [43]. In addition, the calculated nugget geometry at the transverse (YZ) planes agrees well with the corresponding experimental results [29] as shown in Fig. 2(c) and (d) for two different rotation speeds. These agreements indicate that the temperature values calculated using the model can be used for machine learning with confidence.

Although the temperature field can indicate the plasticity of the material around the pin, it does not directly describe the continuity
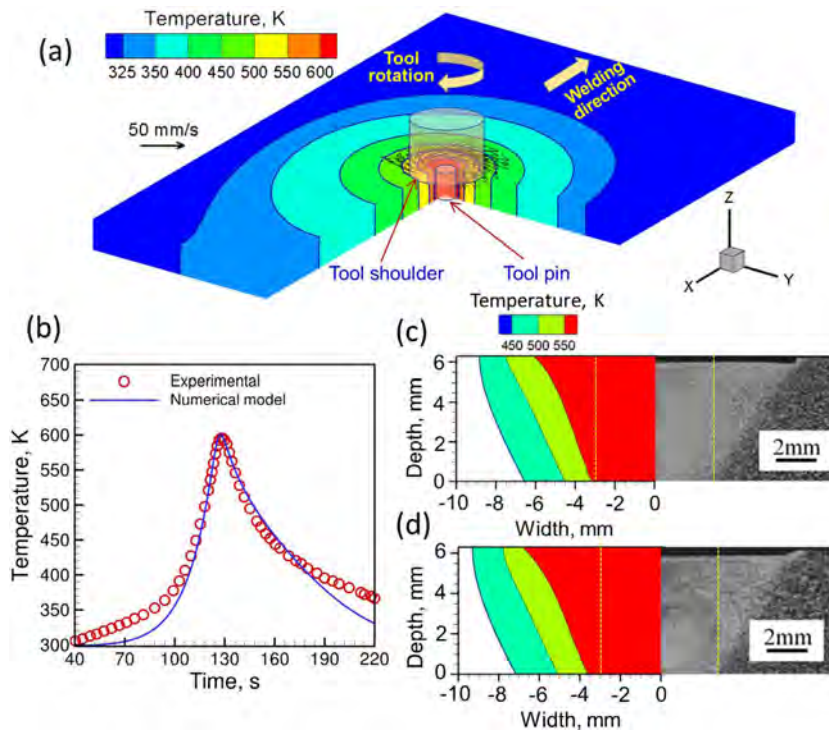
Fig. 2. The schematic of welding process. (a) temperature and velocity fields during FSW of AA2024, welding speed 100 mm/min, rotational speed 800 rpm [43] (b) temperature-time curves from calculation and experimental results, monitor location is 13 mm from welding centerline in advancing side on the top surface of the workpiece [43]. Comparison between the calculated transverse sections of the AA2219 with the corresponding experimentally measured macrographs, rotational speeds are (c) 800 rpm and (d) 1000 rpm, welding speed is 100 mm/min [29]. The yellow dot lines show the edges of the tool pin with radius of 3 mm where the tool pin axis is at width = 0 mm. (For interpretation of the references to colour in this figure legend, the reader is referred to the web version of this article.)

of the flow. Continuity of the material flow around the pin can be represented by the strain rate which is quantified as the spatial gradient of velocity of the flow field. High strain rate may cause discontinuity in the material flow which may result in abrupt load on tool and tool failure [4,5,8]. Strain rate of the plasticized material is affected by the transient velocity distributions around the tool pin. Fig. 3(a) shows the velocity fields around the tool pin at different horizontal (XY) planes. The velocity vectors are represented by the arrows whose magnitudes can be found by comparing their length with the reference vector provided. Since the plasticized material flow is primarily driven by the rotational movement of the shoulder, the magnitudes

Fig. 3. Simulation results from numerical model of (a) velocity field in xy planes of z_1=6.19 mm, z_2=4.34 mm, z_3=2.34 mm from the bottom of the work plate, (b) strain rate (c) flow stress on the tool pin surface. The processing conditions are taken from the literature [43]. The welding speed is 100 mm/min, rotational speed is 800 rpm, diameter of tool pin is 6 mm. 'AS' represeants advancing side while 'RS' represeants retreating side.

of the velocities are the highest near the shoulder (Z_1 plane). However, the magnitudes gradually decrease with the distance from the shoulder. This spatial non-uniformity in the flow field results in strain rate variations as shown in Fig. 3(b). This figure shows the strain rate distribution on the vertical surface of the tool pin. The strain rate at advancing side is higher than that in retreating side, which indicates the discontinuity in flow from the retreating side to the advancing side at the back of the tool pin. This discontinuity may cause abrupt load on tool pin and tool failure in some extreme cases.
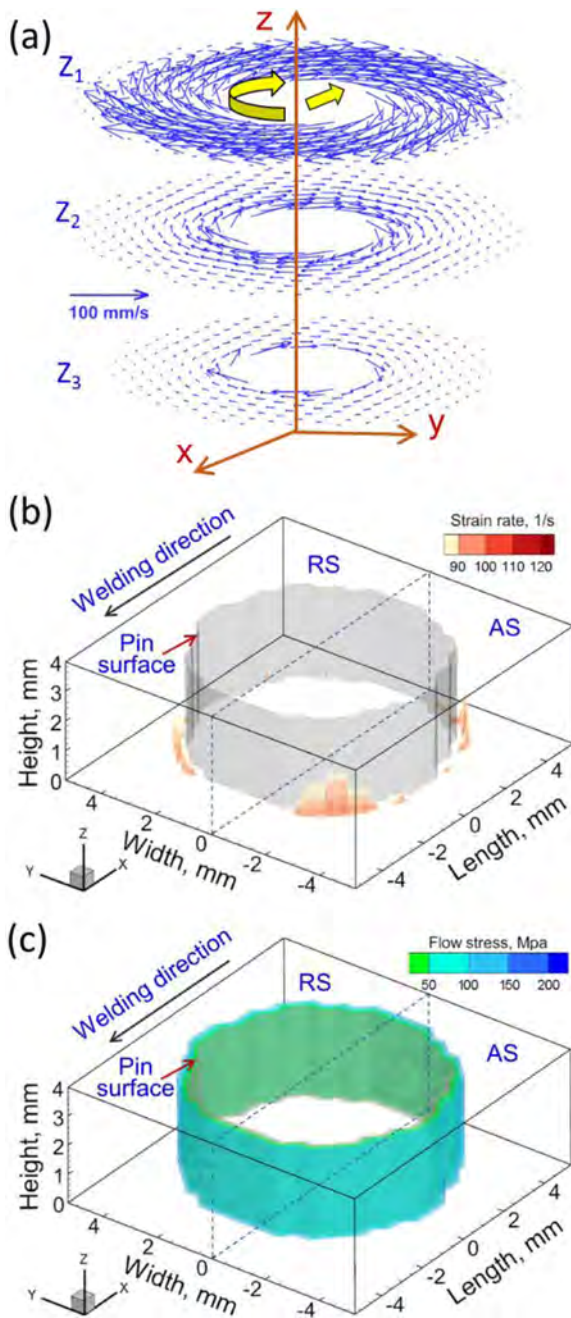
The FSW tools face difficulties in stirring material with high flow stress which may generate high load on the tool pin and result in tool failure. Flow stress is affected by the temperature field as well as the strain rate and thus by the velocity field [2,3]. Since both the temperature and velocity fields are spatially non-uniform, the flow stress field also varies significantly. Fig. 3(c) shows that the flow stress increases with the radial distance from the central axis of the tool pin. The material is easy to flow when the plasticized material is close to the tool pin, and the material which is far from the tool pin is more difficult to flow around. Tool failure is affected by this spatial non-uniformity in flow stress fields.

From the aforementioned discussions, it is evident that the temperature, strain rate and flow stress represent the material flow behavior that has significant effects on tool failure. However, tool failure is also affected by the mechanical loading on the tool represented by the traverse force, torque and shear stress. For example, the tool failure is more likely to happen when the tool pin cannot bear the excessive deformation caused by high traverse force. The traverse force is calculated and compared with corresponding experimental results for different welding conditions for aluminum alloys AA7039 and AA7075 as shown in Fig. 4. The agreement between the computed and measured results provides us the confidence to use these results in machine learning to predict tool failure. Traverse force increases at low heat input, with reduction in rotational speed and increase in welding speed. Tool pin has low load bearing ability because of its smaller diameter than the shoulder. Therefore, the tool pin is more susceptible to suffer from deformation and failure in extreme cases compared to the shoulder [1,5].
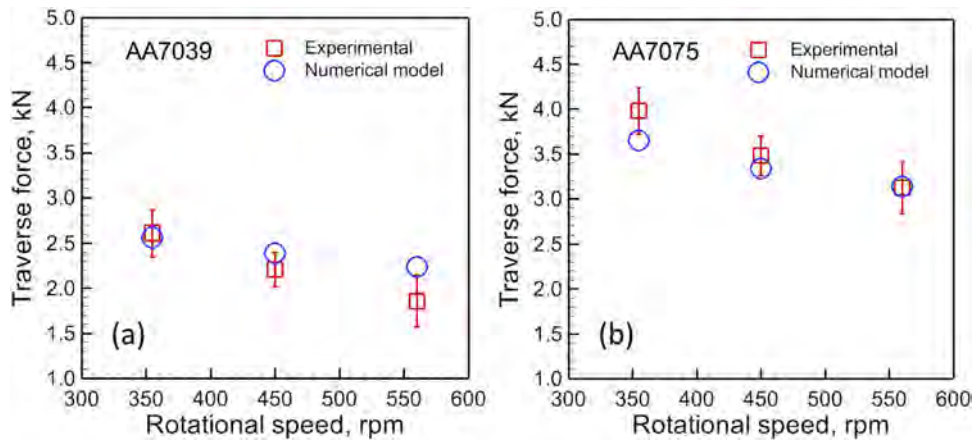
The tool torque indicates the difficulty suffered by the tool to stir the material. The welding conditions that generate high torque on the tool may also cause the separation of different layers of plasticized material resulting in high load on tool and tool failure. The torque is calculated and compared with corresponding experimental results for different welding conditions for aluminum alloys AA7039 and AA7075 as shown in Fig. 5. The agreement between the computed and measured results of tool torque provides us the confidence to use these results in machine learning to predict tool failure. The torque follows the same trend as traverse force which increases at low heat input. More power is required to stir the same amount of material at low temperature, which results in high torque and more deformation and low tool load bearing ability [1,8].

Shear failure of the tool pin may occur if the shear stress on pin exceeds the shear yield strength of the tool pin material. However, the shear stress on the tool pin is non-uniform because it is generated due to a combined effect of bending due to the translation as well as torsion due to rotation of the tool, both of which vary significantly [8]. The non-uniformity of shear stress is evident from Fig. 6 where the variation in shear stress is plotted with the angular distance at a horizontal plane at the mid height of the tool pin. The figure shows that the maximum shear stress is found at the retreating side with 90° from welding direction. This location on the tool pin is the most vulnerable to initiate the shear failure of the pin.
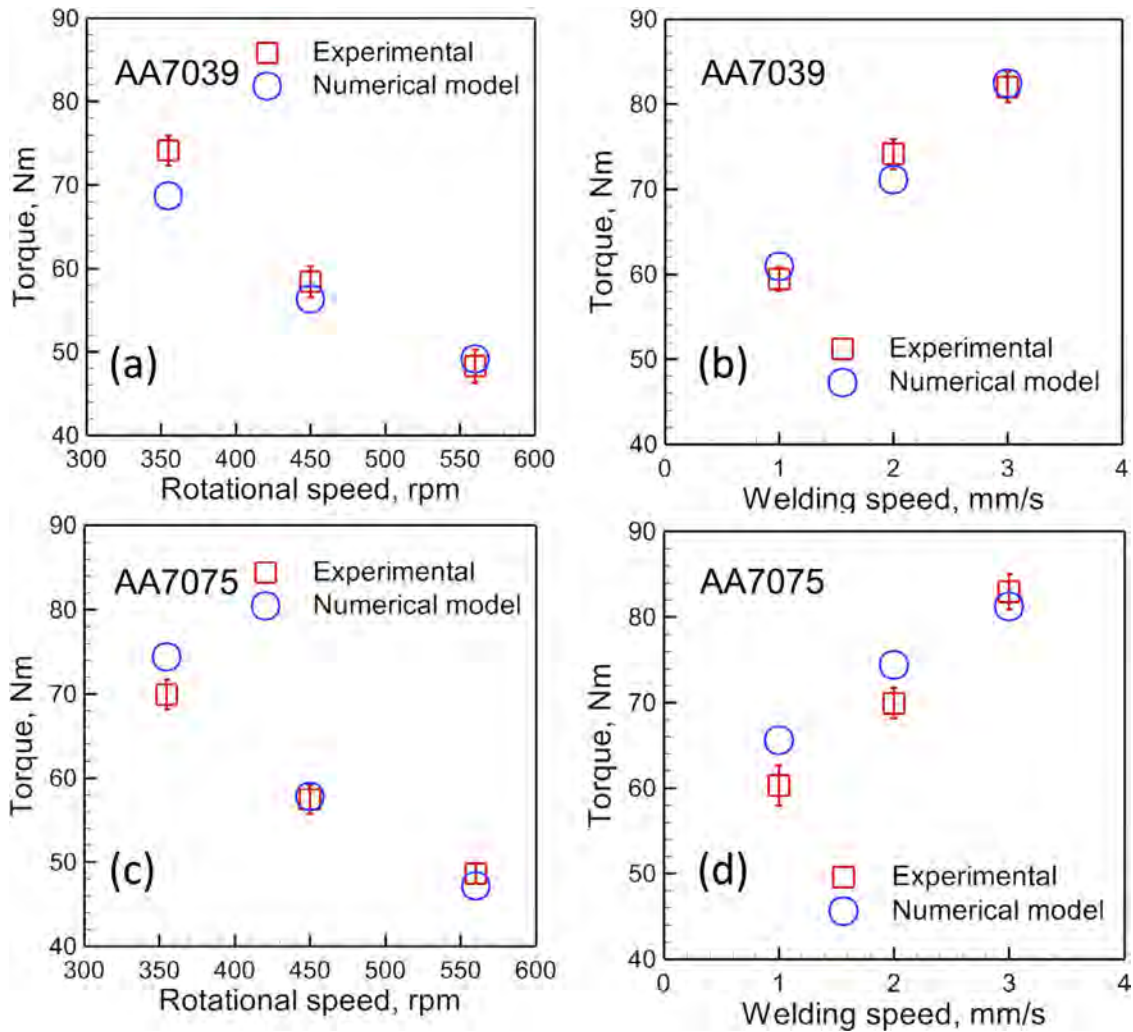
The aforementioned influences of the six causative variables on tool failure are quantitively summarized in Table 1 by considering a simple example [29] of FSW of AA2219. Welds at three different rotational speeds, 2.50, 6.67 and 10.00 rps (revolutions per second) are considered. It was experimentally found that the tool was broken at

Fig. 4. Results of traverse force of experimental measurement and numerical models for with welding speed of 2 mm/s for aluminum alloy (a) AA7039 and (b) AA7075 [44]. The maximum measurement error of the experimental results for traverse force is 0.29 kN.


Fig. 5. Comparing the results of torque on tool pin with experimental measurement and numerical model calculations for different welding conditions (a) AA7039 with constant welding speed of 2 mm/s (b) AA7039 with constant rotational speed of 355 rpm (c) AA7075 with constant welding speed of 2 mm/s (d) AA7075 with constant rotational speed of 355 rpm [44]. The maximum measurement error of the experimental results for torque is 2.0 Nm.

the rotational speed of 2.50 rps. In contrast, tool was safe at higher rotational speeds of 6.67 and 10.00 rps. Six causative variables corresponding to the three welds at different rotational speeds are calculated using the numerical model and provided in the Table 1. It is evident from the table that the tool failure can be avoided at high temperature but low relative stain rate, flow stress, traverse force, torque and maximum shear stress.

Calculations of six causative variables similar to that presented in Table 1 are performed corresponding to one hundred and fourteen experimental cases. The results obtained are used in machine
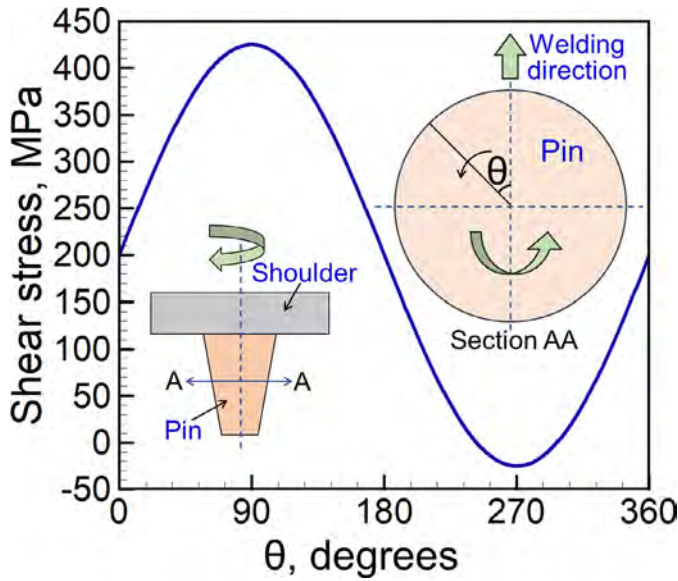
Fig. 6. Shear stress variation with the angular distance of the tool pin, where 0° indicates the welding direction. The values are taken at the mid-height of the tool pin at section AA as schematically represented in the inset. The welding speed is 100 mm/min, rotational speed is 800 rpm. The processing conditions are taken from the literature [43].

Table 2
Range of unprocessed, raw parameters and causative variables.

Unprocessed parameters		Causative variables	
Parameters	Range	Variables	Range
Welding speed, m/s	0.00167−0.0183	Peak temperature, K	441.07−789.93
Rotational speed, rps	2.5−21.7	Strain rate, /s	23.16−434.25
Plate thickness, m	0.003−0.00635	Flow stress, MPa	153.55−629.81
Shoulder radius, m	0.005−0.0105	Traverse force, kN	2.31−11.64
Axial pressure, Mpa	13−122	Torque, N*m	13.80−205.58
Pin root radius, m	0.002−0.0035	Maximum shear stress, MPa	58.74−2666.3
Tilt angle, degree	1−3		
Thermal			

diffusivity, $\times 10^{-5} m^2/s$4.89−7.13Yield strength, Mpa150−352

learning to find the hierarchical influence of the six variables on tool failure as discussed below. The range of unprocessed raw parameters and six causative variables is listed in Table 2. Raw welding parameters, material properties and calculated six causative variables for one hundred and fourteen data points are available in the Supplementary Information.

3.2. Hierarchical influence of six variables on tool failure

The calculated results of six causative variables corresponding to all of the one hundred and fourteen experimental datasets are normalized and plotted in Fig. 7. In order to avoid effects of composition of different aluminum alloys, the data for individual alloy are normalized by dividing each of the six variables by their maximum values. All data used in these plots are provided in the Supplementary Information. These results are used in neural network to evaluate their effectiveness in predicting tool failure. It is found that the accuracy in prediction of tool failure is 96.3% which is higher than the prediction accuracy of 87.0% using the raw welding variables as discussed earlier. Therefore, it is evident that the six causative variables are more effective in forecasting tool failure compared to the raw welding variables.

Receiver operating characteristic (ROC) curve and area under ROC curve (AUC) can show the generalization ability of the model [30]. An ROC curve is a graph showing the performance of a classification model at all classification thresholds. This threshold value is used for the output of neural network to classify the dataset with and without tool broken. The x-axis shows the false positive rate and the y-axis is the true positive rate. Both the false positive rate and true positive rate are explained in the Supplementary Information. The ROC curves of the neural network using both raw welding parameters and causative variables are plotted in Fig. 8. The red dotted line is the ROC curve for random estimations representing a model with 50% accuracy for both '0' and '1'. AUC value is an important index to show the model property. The AUC value is a continuous value between 0 and 1, the greater value indicating better model property, and the curve getting closer to the top left (0,1) point. The curve for causative variable is closer to the (0,1) with AUC of 0.99 comparing to the curve for raw welding parameters with AUC of 0.97. The neural network feeding with causative variables has better generalization ability compared to that with raw welding parameters.

Although these six variables are found to be effective in predicting tool failure, their hierarchical influence on tool failure needs to be evaluated in order to find out which variable among the six should be tuned in first to mitigate tool failure. Three commonly used feature selection indexes are applied to evaluate the feature importance for the six causative variables using all data points, information gain (IG), information gain ratio (IG ratio) and Gini index. The calculated three indexes are plotted in Fig. 9. For IG and IG ratio, the index with highest value has the most importance in classification. It is because both IG and IG ratio are calculated based on entropy, and the highest IG (or IG ratio) with lowest uncertainty of which the corresponding variable is the best for classification. However, for Gini index which

Table 1
Variations in welding parameters and causative variables for different joints. The weld macrographs are taken from literature [29]. Relative strain rate equal to the ratio between the strain rate and the rotation speed in rps.

|	Broken tool	Safe tool	Safe tool
Rotation speed, rps	2.5	6.67	10.00
Peak temp., T_P, K	602.21	678.98	719.74
Relative strain rate, ε_r	2.7	1.5	1.2
Flow stress, τ_f, MPa	150.20	121.10	110.50
Traverse force, F, kN	4.17	2.05	1.41
Torque, M, Nm	43.81	23.60	14.76
Max shear stress, τ_m, MPa	685.5	557.3	503.1
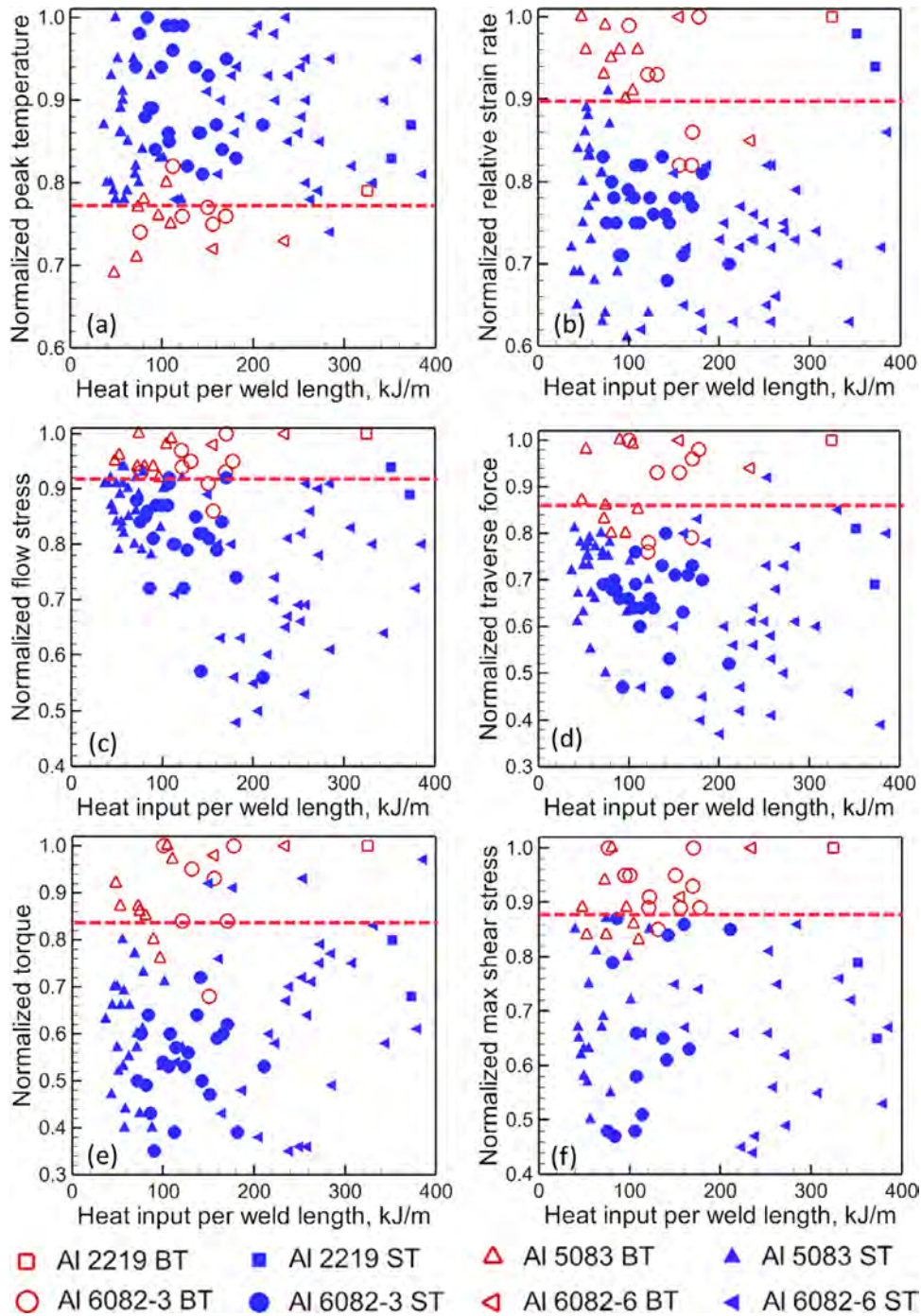
Fig. 7. Normalized calculated results obtained from the numerical model. (a) Peak temperature, (b) relative strain rate (strain rate/rps), (c) flow stress, (d) traverse force, (e) torque, (f) maximum shear stress [29,40,41]. 'BT' represents 'Broken tool', 'ST' represents 'Safe tool'. The AA6082 plates with different thickness of 3 and 6 mm were marked with 'Al 6082-3' and 'Al 6082-6' respectively.

represent the impurity, the variable with the least value has the most influence on data classification. Six causative variables are ranked with these three feature selection indexes and shown in Fig. 9(a), (b) and (c). Three indexes all show that the maximum shear stress and flow stress are the first and second important variables for tool failure, and the peak temperature is the last important variable for tool failure.

We also used the calculated values of six variables to construct a decision tree using three algorithms to predict tool failure. For the decision-making criteria, threshold values for all six variables are needed which classify the welding cases into 'Broken tool' (BT) and 'Safe tool' (ST). The threshold values are indicated by horizontal

dotted lines in Fig. 7. For example, the welds corresponding to the normalized maximum shear stress higher than 0.88 are prone to the tool failure. All three algorithms provided exactly the same decision tree which is shown in Fig. 10. The first and second important variables on tool failure shown in Fig. 9 are selected as the two classified nodes in decision tree plotted in Fig. 10. The maximum shear stress is selected as the root node which is also found as the most important variable for the tool failure as mentioned before. Flow stress is selected to be the classify node in the second-time ranking that is found to be the second important variable that affects tool failure in Fig. 9. The other four variables, peak temperature, relative strain rate, traverse force and torque are found to be the less important variables
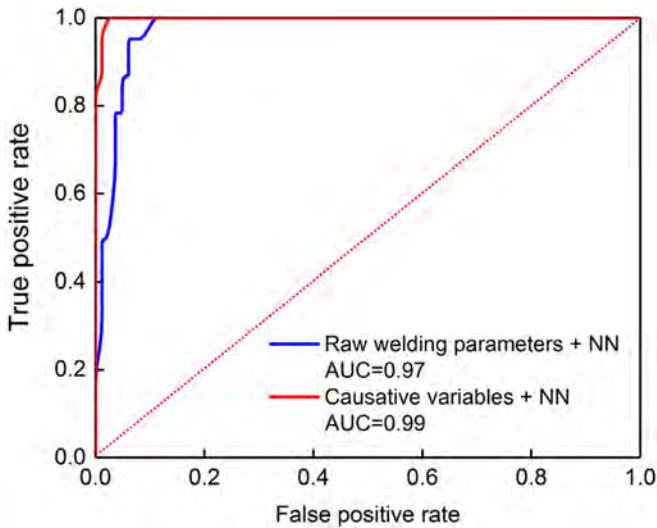
Fig. 8. Receiver operating characteristic (ROC) curves for neural network using raw welding parameters and causative variables. The red dotted line is the ROC curve for random estimations which represents a model with 50% accuracy for both '0' and '1'. ROC curve and area under ROC curve (AUC) can show the generalization ability of the model. The greater AUC value indicates the curve closer to the top left (1,0) point and better prediction ability of the neural network. (For interpretation of the references to colour in this figure legend, the reader is referred to the web version of this article.)

and not selected as nodes in the decision tree, since the influence of these four variables are included in the maximum shear stress on the tool pin and flow stress of the plasticized material.

The decision tree can predict tool failure if the values of the causative variables are known. It is found that the decision tree constructed here (shown in Fig. 10) can predict tool failure with an accuracy of 98.1% which is better than that using neural network. Therefore, use of both neural network and decision tree based on the causative variables are better than using raw variables in predicting tool failure. This is also evident from the corresponding confusion matrices [30,31] as shown in Fig. 11. The confusion matrix is applied to show the comparison between the predicted results and the target output for each method. Fig. 11(a) explains the basic structure of the confusion matrix. The result of the neural network using raw welding parameters is shown in Fig. 11(b), with an accuracy of 87.0%. The results using the causative variables for neural network and decision tree are shown in Fig. 11(c) and (d), with accuracy of 96.3% and 98.1% respectively. The accuracy, sensitivity and specificity of the three methods are summarized in Table 3. Calculations of the accuracy, sensitivity and specificity are explained in the Supplementary Information.

4. Summary and conclusions

One hundred and fourteen experimental data sets for three aluminum alloys, AA2219, AA5083 and AA6061 were used to identify six causative variables for tool failure in friction stir welding. The six variables, temperature, traverse force, maximum shear stress, flow stress, strain rate and torque are calculated using a well-tested heat transfer and material flow model. Three different decision tree-based algorithms are used to rank these variables based on their hierarchical influence on tool failure. Below are the specific findings.

(1) Temperature, traverse force, maximum shear stress, flow stress, strain rate and torque could be correlated with tool failure based on a neural network. The neural network could predict tool failure with a high level of confidence.
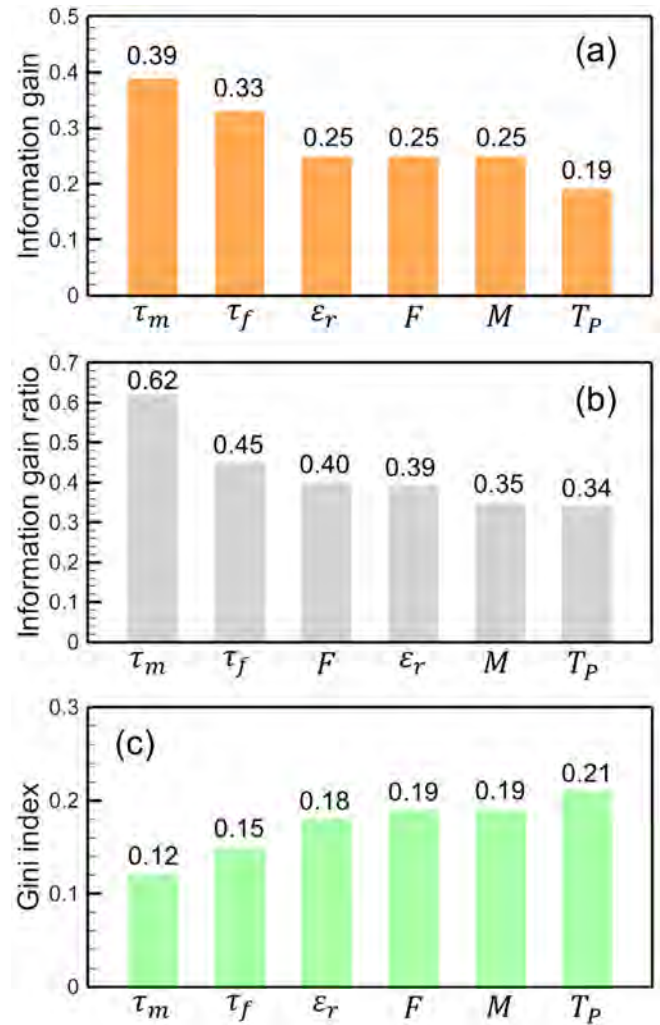
Fig. 9. Results of three feature selection indexes of (a) information gain, (b) information gain ratio, and (c) Gini index for six normalized causative variables. These three indexes indicate the feature importance. For each index, the hierarchical importance of these six causative variables on tool failure is ranked and shown in this figure. For all three algorithms, maximum shear stress (τ_m) and flow stresses (τ_f) have been found to be the two most important variables. However, all three algorithms show that the peak temperature (T_P) has the least influence on tool failure.
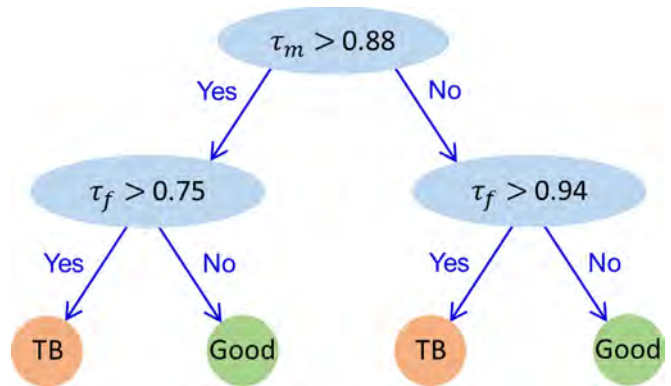
Fig. 10. Decision tree with six normalized causative variables for tool breakage classification. 'TB' represents the conditions for which tools are broken. 'Good' represents the safe conditions for which tools are not broken. The maximum shear stress (τ_m) and flow stress (τ_f) are determined as the variables for classification in the decision tree.
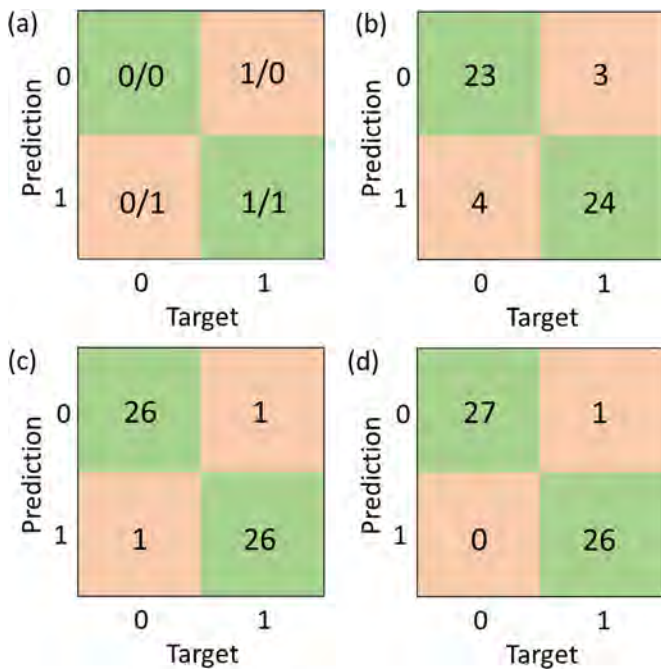
Fig. 11. Confusion matrices that compare the predicted output from the machine learning and the target output obtained from the 114 experimental data, assigning '1' for 'Broken tool' and '0' for 'Safe tool'. (a) The basic construction of a confusion matrix, results of (b) raw welding parameters using neural network, accuracy=87.0%, (c) causative variables using neural network, accuracy=96.3% and (d) causative variables using decision tree, accuracy=98.1%. (For interpretation of the references to colour in this figure legend, the reader is referred to the web version of this article.)

Table 3

Accuracy, sensitivity and specificity of three methods (1) raw welding parameters using neural network, (2) causative variables using neural network and (3) causative variables using decision tree.

	Method 1	Method 2	Method 3
Accuracy	87.0%	96.3%	98.1%
Sensitivity	88.9%	96.3%	96.3%
Specificity	85.2%	96.3%	100.0%

(2) The most important variables for tool failure are found to be maximum shear stress and flow stress in the order of importance. The maximum shear stress combines the complicated influence of bending and torsion stresses on the tool pin and is an important factor which can cause tool failure. High flow stress indicates the difficulty in material flow around the tool pin and may result in high load on tool. Peak temperature is the least important variable among the six causative variables. Three decision tree-based algorithms predicted the same hierarchy and forecasted the tool failure with an accuracy of 98%.

(3) The six computed causative variables are better than the raw, unprocessed welding variables at forecasting tool failure. The neural network fed with welding parameters, tool and work plate dimensions and material properties can predict tool failure with 87.0% accuracy. In contrast, the neural network using the causative variables can forecast tool failure with a 96% accuracy.

(4) Local discontinuity in the flow field of the plasticized material due to low peak temperature and high strain rate may cause abrupt load on the tool which may result in its failure. Traverse force and torque are indicators of the difficulty in linear movement of the tool and the smooth flow of the plasticized material, respectively.

Declaration of Competing Interest

None.

Supplementary materials

Supplementary material associated with this article can be found, in the online version at doi:10.1016/j.actamat.2020.03.047.

References

[1] R. Nandan, T. DebRoy, H.K.D.H. Bhadeshia, Recent advances in friction-stir welding−process, weldment structure and properties, Prog. Mater. Sci. 53 (2008) 980−1023.

[2] R. Nandan, G.G. Roy, T.J. Lienert, T. Debroy, Three-dimensional heat and material flow during friction stir welding of mild steel, Acta Mater. 55 (2007) 883−895.

[3] A. Arora, T. DebRoy, H.K.D.H. Bhadeshia, Back-of-the-envelope calculations in friction stir welding - velocities, peak temperature, torque, and hardness, Acta Mater. 59 (2011) 2020−2028.

[4] Y. Du, T. Mukherjee, T. DebRoy, Conditions for void formation in friction stir welding from machine learning, Npj Comput. Mater. 5 (2019) doi:10.1038/s41524-019-0207-y. Article no. 68.

[5] R. Rai, A. De, H.K.D.H. Bhadeshia, T. DebRoy, Friction stir welding tools, Sci. Technol. Weld. Joi. 16 (2011) 325−342.

[6] R.S. Mishra, Z.Y. Ma, Friction stir welding and processing, Mater. Sci. Eng. R 50 (2005) 1−78.

[7] F.C. Liu, Y. Hovanski, M.P. Miles, C.D. Sorensen, T.W. Nelson, A review of friction stir welding of steels: tool, material flow, microstructure, and properties, J. Mater. Sci. Technol 34 (2018) 39−57.

[8] A. Arora, M. Mehta, A. De, T. DebRoy, Load bearing capacity of tool pin during friction stir welding, Int. J. Adv. Manuf. Tech. 61 (2012) 911−920.

[9] C.T. Collier, Tool Material Degradation Due to Friction Stir Welding of Aluminum Alloys. Master's thesis. University of South Carolina, Columbia, 2015.

[10] S.R. Nathan, S. Malarvizhi, V. Balasubramanian, A.G. Rao, Failure analysis of tungsten based tool materials used in friction stir welding of high strength low alloy steels, Eng. Fail. Anal. 66 (2016) 88−98.

[11] B.T. Thompson, Tool degradation characterization in the friction stir welding of hard metals, The Ohio State University, Columbus, 2010.

[12] S. Mironov, Y.S. Sato, H. Kokawa, Influence of welding temperature on material flow during friction stir welding of AZ31 magnesium alloy, Metall. Mater. Trans. A. 50 (2019) 2798−2806.

[13] T.F. Flint, J.A. Francis, M.C. Smith, A semi-analytical solution for the transient temperature field generated by a volumetric heat source developed for the simulation of friction stir welding, Int. J. Therm. Sci. 138 (2019) 586−595.

[14] Y. Du, H. Li, L.J. Yang, C.G. Luo, Accurate measurement of residual stress of 2219-T87 aluminum alloy friction stir welding joints based on properties of joints, J. Mech. Sci. Technol. 32 (2018) 139−147.

[15] Y.B. Zhong, C.S. Wu, G.K. Padhy, Effect of ultrasonic vibration on welding load, temperature and material flow in friction stir welding, J. Mater. Process. Tech. 239 (2017) 273−283.

[16] A. Arora, Z. Zhang, A. De, T. DebRoy, Strains and strain rates during friction stir welding, Scripta Mater. 61 (2009) 863−866.

[17] N.Z. Khan, D. Bajaj, A.N. Siddiquee, Z.A. Khan, M.H. Abidi, U. Umer, H. Alkhalefah, Investigation on effect of strain rate and heat generation on traverse force in fsw of dissimilar aerospace grade aluminium alloys, Materials (Basel) 12 (2019) 1641.

[18] W. Xu, H. Wang, Y. Luo, W. Li, M.W. Fu, Mechanical behavior of 7085-T7452 aluminum alloy thick plate joint produced by double-sided friction stir welding: effect of welding parameters and strain rates, J. Manuf. Process. 35 (2018) 261−270.

[19] E. Sharghi, A. Farzadi, Simulation of strain rate, material flow, and nugget shape during dissimilar friction stir welding of AA6061 aluminum alloy and al-mg2si composite, J. Alloy. Compd. 748 (2018) 953−960.

[20] T.U. Seidel, A.P. Reynolds, Visualization of the material flow in AA2195 friction-stir welds using a marker insert technique, Metall. Mater. Trans. A. 32 (2001) 2879−2884.

[21] K.S.V.K. Kumar, S.V. Kailas, The role of friction stir welding tool on material flow and weld formation, Mat. Sci. Eng. A. 485 (2008) 367−374.

[22] P.A. Colegrove, H.R. Shercliff, 3-Dimensional CFD modelling of flow round a threaded friction stir welding tool profile, J. Mater. Process. Tech. 169 (2005) 320−327.

[23] A. Arora, R. Nandan, A.P. Reynolds, T. DebRoy, Torque, power requirement and stir zone geometry in friction stir welding through modeling and experiments, Scr. Mater. 60 (2009) 13−16.

[24] H. Su, C.S. Wu, A. Pittner, M. Rethmeier, Simultaneous measurement of tool torque, traverse force and axial force in friction stir welding, J. Manuf. Process. 15 (2013) 495–500.

[25] M. Mehta, K. Chatterjee, A. De, Monitoring torque and traverse force in friction stir welding from input electrical signatures of driving motors, Sci. Technol. Weld. Joi. 18 (2013) 191–197.

[26] S.D. Ji, Q. Wen, Z.W. Li, A novel friction stir diffusion bonding process using convex-vortex pin tools, J. Mater. Sci. Technol. (2020), doi: 10.1016/j.jmst.2020.01.042.

[27] B. Das, S. Pal, S. Bag, Torque based defect detection and weld quality modelling in friction stir welding process, J. Manuf. Process. 27 (2017) 8–17.

[28] N. Dialami, M. Cervera, M. Chiumenti, C.A. de Saracibar, A fast and accurate two-stage strategy to evaluate the effect of the pin tool profile on metal flow, torque and forces in friction stir welding, Int. J. Mech. Sci. 122 (2017) 215–227.

[29] H. Doude, J. Schneider, B. Patton, S. Stafford, T. Waters, C. Varner, Optimizing weld quality of a friction stir welded aluminum alloy, J. Mater. Process. Tech. 222 (2015) 188–196.

[30] T.M. Mitchell, Machine Learning, McGraw-Hill Science, Portland, OR, USA, 1997.

[31] B. Medasani, A. Gamst, H. Ding, W. Chen, K.A. Persson, M. Asta, A. Canning, M. Haranczyk, Predicting defect behavior in B2 intermetallics by merging ab initio modeling and machine learning, npj Comput. Mater. 2 (2016) 1.

[32] A. Rovinelli, M.D. Sangid, H. Proudhon, W. Ludwig, Using machine learning and a data-driven approach to identify the small fatigue crack driving force in polycrystalline materials, npj Comput. Mater. 4 (2018) 35.

[33] C. Wen, Y. Zhang, C. Wang, D. Xue, Y. Bai, S. Antonov, L. Dai, T. Lookman, Y. Su, Machine learning assisted design of high entropy alloys with desired property, Acta Mater. 170 (2019) 109–117.

[34] J.A. Gomberg, A.J. Medford, S.R. Kalidindi, Extracting knowledge from molecular mechanics simulations of grain boundaries using machine learning, Acta Mater. 133 (2017) 100–108.

[35] A. Rahnama, S. Clark, S. Sridhar, Machine learning for predicting occurrence of interphase precipitation in HSLA steels, Comp. Mater. Sci. 154 (2018) 169–177.

[36] M.H. Shojaeefard, M. Akbari, P. Asadi, Multi objective optimization of friction stir welding parameters using FEM and neural network, Int. J. Precis. Eng. Man. 15 (2014) 2351–2356.

[37] V.D. Manvatkar, A. Arora, A. De, T. DebRoy, Neural network models of peak temperature, torque, traverse force, bending stress and maximum shear stress during friction stir welding, Sci. Technol. Weld. Joi. 17 (2012) 460–466.

[38] H.K.D.H. Bhadeshia, Neural networks in materials science, ISIJ Int. 39 (1999) 966–979.

[39] R.B. Bird, W.E. Stewart, E.N. Lightfoot, Transport Phenomena, John Wiley & Sons, New York, 2006.

[40] R. Louro, C. Leitão, H. Gouveia, A. Loureiro, D.M. Rodrigues, Taguchi analysis of the effect of process parameters in friction stir welding, Mater. Sci. Forum. 636 (2010) 1150–1156.

[41] D.M. Rodrigues, C. Leitao, R. Louro, H. Gouveia, A. Loureiro, High speed friction stir welding of aluminium alloys, Sci. Tech. Weld. Joi. 15 (2010) 676–681.

[42] R. Nandan, G.G. Roy, T. Debroy, Numerical simulation of three-dimensional heat transfer and plastic flow during friction stir welding, Metall. Mater. Trans. A. 37 (2006) 1247–1259.

[43] Y. Zhu, G. Chen, Q. Chen, G. Zhang, Q. Shi, Simulation of material plastic flow driven by non-uniform friction force during friction stir welding and related defect prediction, Mater. Design. 108 (2016) 400–410.

[44] V. Buchibabu, G.M. Reddy, A. De, Probing torque, traverse force and tool durability in friction stir welding of aluminum alloys, J. Mater. Process. Tech. 241 (2017) 86–92.